INT. J. REMOTE SENSING, 2003, VOL. 24, NO. 17, 3503–3514

# Correcting satellite imagery for the variance of reflectance and illumination with topography

J. D. SHEPHERD* and J. R. DYMOND
Landcare Research, Palmerston North, New Zealand

(*Received 23 October 2000; in final form 15 March 2002*)

**Abstract.** Steephill and mountain slopes severely affect remote sensing of vegetation. The irradiation on a slope varies strongly with slope azimuth relative to the sun, and the reflectance of the slope varies with the angles of incidence and exitance relative to the slope normal. Topographic correction involves standardizing imagery for these two effects. We use an atmospheric model with a Digital Elevation Model (DEM) to calculate direct and diffuse illumination, and a simple function of incidence and exitance angles to calculate vegetation-canopy reflectance on terrain slope. The reflectance correction has been derived from the physics of visible direct radiation on a vegetation canopy, but has proved applicable to infrared wavelengths and only requires solar position, slope and aspect. We applied the reflectance and illumination correction to a SPOT 4 image of New Zealand to remove topographic variation. In all spectral bands, the algorithm markedly reduced the coefficients of variation of vegetation groups on rugged terrain. This produced clean spectral signatures, improving the capacity for automated classification. If illumination correction is performed alone, the coefficients of variation can be increased, and so should not be applied without a reflectance correction. The algorithm output is reflectance on a level surface, enabling the monitoring of vegetation in hilly and mountainous areas.

## 1. Introduction

The effect of topography on radiance in optical satellite imagery has long been recognized (Stohr and West 1975, Holben and Justice 1980, Leprieur *et al.* 1988, Thomson and Jones 1990). Slopes facing toward the sun receive more light and appear brighter than slopes facing away from the sun. Not only is illumination modified by topography, but the proportion of light reflected toward the satellite also varies with the geometry of sun, target and viewer; and this geometry varies with topography (Teillet *et al.* 1982, Hugli and Frei 1983). In order to maximize the information content in satellite imagery of hilly or mountainous areas, it is necessary to remove, or account for, the effect of topography (Teillet 1986).

A variety of approaches have been tried. Image analysis solutions attempt to account for topography in the interpretation stage (Fleming and Hoffer 1979, Hutchinson 1982, Franklin *et al.* 1989, Dymond 1992, Conese *et al.* 1993b). These methods generally require much training data and are unable to disentangle the

*e-mail: shepherdj@landcare.cri.nz

*International Journal of Remote Sensing*
ISSN 0143-1161 print/ISSN 1366-5901 online © 2003 Taylor & Francis Ltd
http://www.tandf.co.uk/journals
DOI: 10.1080/01431160210154029

geometric topographic effect, described above, from the effect of topography on the geographic distribution of vegetation (with the exception of Conese *et al.* (1993b) who used a principal component transformation). The cosine correction assumes the Lambert law of reflection and models solely the variation of illumination with topography (Roberts 1981, Woodham and Gray 1987, Proy *et al.* 1989, Senoo *et al.* 1990, Conese *et al.* 1993a, Pellikka 1996, Richter 1997, Sandmeier and Itten 1997). However, several authors have found this method actually increases scene variance (Teillet *et al.* 1982, Civco 1989, Meyer *et al.* 1993). Empirical correction methods model the variation of illumination and reflection together through functions of arbitrary parameters (Smith *et al.* 1980, Justice *et al.* 1981, Dymond 1988, Meyer *et al.* 1993, Ekstrand 1996, Trotter 1998). Because the range of model validity is uncertain, parameter fitting is required for each scene.

Recently, the effect of topography on reflectance has been characterized (Dymond and Shepherd 1999). This permits illumination and reflectance correction together. In this paper, we use the 6S atmospheric correction code of Vermote *et al.* (1997), the illumination correction of Sandmeier and Itten (1997), and the reflectance correction of Dymond and Shepherd (1999) to provide a full physically modelled correction of the topographic effect. We then use a 20 m resolution Digital Elevation Model (DEM) to correct the topographic effect in a SPOT4 scene of a mountainous area in the South Island of New Zealand. Finally, we quantify the reduction in scene variance brought about by the topographic correction and compare this with only performing illumination (or Lambertian) correction.

## 2. Methods

### 2.1. *Irradiance calculation*

To correct the varying illumination of terrain, it is necessary to model the radiation field reaching a sloping surface. For this study the transmission model used was the Second Simulation of the Satellite Signal in the Solar Spectrum (6S) (Vermote *et al.* 1997). This software predicts the direct and diffuse irradiance from a cloudless sky onto a horizontal surface at a given altitude. The spectral range of the model is from 0.25 to 4.0 $\mu$m. Atmospheric processes considered in the 6S code are gaseous absorption and scattering by molecules and aerosols.

To generalize the horizontal surface predictions of 6S to a sloping surface we simplify the formulation of Sandmeier and Itten (1997), and write the total solar irradiance $E(b, z)$ on a sloping surface as

$$E(b, z) = \Theta E_{\mathrm{h}}^{\mathrm{dir}}(b, z)\frac{\cos i}{\cos i_{\mathrm{h}}} + E_{\mathrm{h}}^{\mathrm{dif}}(b, z)V_{\mathrm{d}} + E_{\mathrm{h}}(b, z)V_{\mathrm{t}}\rho_{\mathrm{adj}}(b) \tag{1}$$

where $b$, spectral band; $z$, altitude; $E$, total irradiance on a sloping surface; $E_{\mathrm{h}}$, total irradiance on a horizontal surface; $E_{\mathrm{h}}^{\mathrm{dir}}$, direct component of irradiance on a horizontal surface; $E_{\mathrm{h}}^{\mathrm{dif}}$, diffuse component of irradiance on a horizontal surface; $\Theta$, binary coefficient, set to zero in cast shadow; $i$, incidence angle between the surface normal and the sun; $i_{\mathrm{h}}$, incidence angle for horizontal surface (solar zenith angle); $V_{\mathrm{d}}$, sky-view factor; $V_{\mathrm{t}}$, terrain-view factor; and $\rho_{\mathrm{adj}}$, average reflectance of adjacent objects.

The first term in equation (1) is the cosine law for direct radiation, set to zero in areas of cast shadow. The second term describes the diffuse irradiance, where the diffuse light from the isotropic sky is weighted by the fraction of sky seen, $V_{\mathrm{d}}$, which

Table 1. Statistics of the 12 unsupervised clusters for the green spectral band of SPOT 4. $\bar{s}$ is the average slope of the cluster, $V_a$ is the coefficient of variation (%) of green reflectance in the original atmosphere-corrected imagery, $V_b$ is the coefficient of variation (%) of green reflectance after full correction for illumination and directional reflectance, $V_c$ is the coefficient of variation (%) of green reflectance after only illumination (or Lambertian) correction, $\Delta V_{ab}$ is the change in coefficient of variation for full reflectance correction, and $\Delta V_{ac}$ is the change in coefficient of variation for illumination correction.

| Cluster | Cover | Area (km$^2$) | $\bar{s}$ (°) | $V_a$ | $V_b$ | $V_c$ | $\Delta V_{ab}$ (%) | $\Delta V_{ac}$ (%) |
|---|---|---|---|---|---|---|---|---|
| 1 | Forest | 92.2 | 25.1 | 20.2 | 16.5 | 21.7 | −18 | 7 |
| 2 | Forest | 104.8 | 26.1 | 17.6 | 14.1 | 21.0 | −20 | 19 |
| 3 | Forest | 51.2 | 25.2 | 18.9 | 17.0 | 25.3 | −10 | 34 |
| 4 | Shrub | 71.7 | 25.2 | 22.7 | 17.1 | 22.8 | −25 | 0 |
| 5 | Shrub | 35.8 | 26.3 | 27.6 | 25.0 | 29.3 | −9 | 6 |
| 6 | Bare | 24.6 | 25.3 | 22.5 | 14.4 | 19.2 | −36 | −15 |
| 7 | Bare | 30.5 | 26.0 | 23.3 | 15.0 | 18.9 | −36 | −19 |
| 8 | Tussock | 89.6 | 21.6 | 19.8 | 15.6 | 20.5 | −21 | 4 |
| 9 | Tussock | 84.6 | 21.6 | 19.3 | 16.1 | 22.6 | −17 | 17 |
| 10 | Tussock | 74.3 | 13.8 | 13.1 | 10.5 | 13.6 | −20 | 4 |
| 11 | Pasture | 25.1 | 5.6 | 16.9 | 17.8 | 22.8 | 5 | 35 |
| 12 | Pasture | 40.8 | 2.9 | 20.9 | 20.7 | 21.1 | −1 | 1 |

Table 2. Statistics of the 12 unsupervised clusters for the red spectral band of SPOT 4. $\bar{s}$ is the average slope of the cluster, $V_a$ is the coefficient of variation (%) of red reflectance in the original atmosphere-corrected imagery, $V_b$ is the coefficient of variation (%) of red reflectance after full correction for illumination and directional reflectance, $V_c$ is the coefficient of variation (%) of red reflectance after only illumination (or Lambertian) correction, $\Delta V_{ab}$ is the change in coefficient of variation for full reflectance correction, and $\Delta V_{ac}$ is the change in coefficient of variation for illumination correction.

| Cluster | Cover | Area (km$^2$) | $\bar{s}$ (°) | $V_a$ | $V_b$ | $V_c$ | $\Delta V_{ab}$ (%) | $\Delta V_{ac}$ (%) |
|---|---|---|---|---|---|---|---|---|
| 1 | Forest | 92.2 | 25.1 | 22.3 | 19.3 | 24.3 | −13 | 9 |
| 2 | Forest | 104.8 | 26.1 | 20.8 | 18.1 | 24.2 | −13 | 16 |
| 3 | Forest | 51.2 | 25.2 | 25.3 | 23.6 | 30.5 | −7 | 21 |
| 4 | Shrub | 71.7 | 25.2 | 24.7 | 19.2 | 24.5 | −22 | −1 |
| 5 | Shrub | 35.8 | 26.3 | 30.4 | 27.8 | 32.1 | −9 | 6 |
| 6 | Bare | 24.6 | 25.3 | 22.5 | 13.7 | 18.8 | −39 | −16 |
| 7 | Bare | 30.5 | 26.0 | 22.8 | 13.8 | 17.5 | −39 | −23 |
| 8 | Tussock | 89.6 | 21.6 | 19.9 | 15.2 | 19.9 | −24 | 0 |
| 9 | Tussock | 84.6 | 21.6 | 20.3 | 16.7 | 22.7 | −18 | 12 |
| 10 | Tussock | 74.3 | 13.8 | 13.5 | 10.7 | 13.3 | −21 | −1 |
| 11 | Pasture | 25.1 | 5.6 | 22.1 | 22.9 | 27.2 | 4 | 23 |
| 12 | Pasture | 40.8 | 2.9 | 19.7 | 19.4 | 19.7 | −2 | 0 |

is approximated by a trigonometric function (Kondratyev 1969)

$$V_{\mathrm{d}} = \frac{1+\cos s}{2} \tag{2}$$

where $s$ is the slope angle. The third term in equation (1) describes the terrain irradiance, radiation that has been reflected from neighbouring slopes, which are considered Lambertian with average reflectance $\rho_{\mathrm{adj}}$. The terrain irradiance is weighted for the fraction of terrain seen, $V_{\mathrm{t}}$, which is approximated in a similar

Table 3. Statistics of the 12 unsupervised clusters for the near-infrared spectral band of SPOT 4. $\bar{s}$ is the average slope of the cluster, $V_a$ is the coefficient of variation (%) of near-infrared reflectance in the original atmosphere-corrected imagery, $V_b$ is the coefficient of variation (%) of near-infrared reflectance after full correction for illumination and directional reflectance, $V_c$ is the coefficient of variation (%) of near-infrared reflectance after only illumination (or Lambertian) correction, $\Delta V_{ab}$ is the change in coefficient of variation for full reflectance correction, and $\Delta V_{ac}$ is the change in coefficient of variation for illumination correction.

| Cluster | Cover | Area (km$^2$) | $\bar{s}$ (°) | $V_a$ | $V_b$ | $V_c$ | $\Delta V_{ab}$ (%) | $\Delta V_{ac}$ (%) |
|---|---|---|---|---|---|---|---|---|
| 1 | Forest | 92.2 | 25.1 | 16.0 | 5.3 | 11.3 | −67 | −29 |
| 2 | Forest | 104.8 | 26.1 | 16.6 | 3.9 | 11.8 | −77 | −29 |
| 3 | Forest | 51.2 | 25.2 | 17.5 | 5.5 | 13.0 | −69 | −26 |
| 4 | Shrub | 71.7 | 25.2 | 17.7 | 9.9 | 15.9 | −44 | −10 |
| 5 | Shrub | 35.8 | 26.3 | 19.3 | 13.5 | 18.5 | −30 | −4 |
| 6 | Bare | 24.6 | 25.3 | 22.0 | 13.4 | 18.4 | −39 | −16 |
| 7 | Bare | 30.5 | 26.0 | 19.8 | 10.6 | 16.0 | −46 | −19 |
| 8 | Tussock | 89.6 | 21.6 | 14.7 | 7.4 | 12.6 | −50 | −14 |
| 9 | Tussock | 84.6 | 21.6 | 13.8 | 6.5 | 12.5 | −53 | −9 |
| 10 | Tussock | 74.3 | 13.8 | 10.9 | 8.3 | 10.7 | −24 | −2 |
| 11 | Pasture | 25.1 | 5.6 | 11.8 | 9.4 | 10.4 | −20 | −12 |
| 12 | Pasture | 40.8 | 2.9 | 10.7 | 10.2 | 10.3 | −5 | −4 |

Table 4. Statistics of the 12 unsupervised clusters for the mid-infrared spectral band of SPOT 4. $\bar{s}$ is the average slope of the cluster, $V_a$ is the coefficient of variation (%) of mid-infrared reflectance in the original atmosphere-corrected imagery, $V_b$ is the coefficient of variation (%) of mid-infrared reflectance after full correction for illumination and directional reflectance, $V_c$ is the coefficient of variation (%) of mid-infrared reflectance after only illumination (or Lambertian) correction, $\Delta V_{ab}$ is the change in coefficient of variation for full reflectance correction, and $\Delta V_{ac}$ is the change in coefficient of variation for illumination correction.

| Cluster | Cover | Area (km$^2$) | $\bar{s}$ (°) | $V_a$ | $V_b$ | $V_c$ | $\Delta V_{ab}$ (%) | $\Delta V_{ac}$ (%) |
|---|---|---|---|---|---|---|---|---|
| 1 | Forest | 92.2 | 25.1 | 18.0 | 11.3 | 16.1 | −37 | −11 |
| 2 | Forest | 104.8 | 26.1 | 16.5 | 9.6 | 16.0 | −42 | −3 |
| 3 | Forest | 51.2 | 25.2 | 19.8 | 13.4 | 18.8 | −32 | −5 |
| 4 | Shrub | 71.7 | 25.2 | 18.9 | 9.6 | 12.7 | −49 | −33 |
| 5 | Shrub | 35.8 | 26.3 | 20.6 | 13.0 | 16.0 | −37 | −22 |
| 6 | Bare | 24.6 | 25.3 | 19.6 | 11.1 | 17.1 | −43 | −13 |
| 7 | Bare | 30.5 | 26.0 | 19.0 | 9.3 | 12.8 | −51 | −33 |
| 8 | Tussock | 89.6 | 21.6 | 15.2 | 7.5 | 9.9 | −51 | −35 |
| 9 | Tussock | 84.6 | 21.6 | 16.0 | 8.2 | 11.4 | −49 | −29 |
| 10 | Tussock | 74.3 | 13.8 | 11.4 | 6.9 | 7.4 | −39 | −35 |
| 11 | Pasture | 25.1 | 5.6 | 16.4 | 14.6 | 15.2 | −11 | −7 |
| 12 | Pasture | 40.8 | 2.9 | 8.2 | 7.1 | 7.0 | −13 | −15 |

manner to equation (2)

$$V_t = \frac{1-\cos s}{2} \tag{3}$$

Equations (1)–(3) along with a DEM enable calculation of the total irradiance onto a landscape from the horizontal surface values obtained from 6S. The only external

term required is the average surface reflectance, $\rho_{adj}(b)$, which can be estimated from the mean atmosphere-corrected reflectances of the chosen satellite image.

Implementation of the irradiance calculation involved initializing 6S with a monthly climatological mean profile of pressure, temperature, water vapour and ozone, obtained by ozonesonde by the National Institute of Water and Atmosphere Research (NIWA). The model was then run for the view and solar angles that correspond with the imagery, at 200 m elevation steps from sea level to the maximum altitude present in the DEM file. An altitude Look Up Table (LUT) of all the horizontal surface values required for equation (1) is then produced for each spectral band. A cast shadow algorithm is run across the DEM for the solar position of image acquisition, to produce a binary shadow mask ($\Theta$). The DEM is also used to calculate slope $s$, and incidence angle $i$. These data layers are combined to evaluate equation (1) for the entire DEM by linear interpolation within the altitude LUT of 6S horizontal surface values. The output is two irradiance images per spectral band, one for direct light ($E^{dir}$) and one for diffuse light ($E^{dif}$). Examples of these for the SPOT 4 image extract used in this study are shown in figure 1.

### 2.2. *Reflectance correction*

The general equation for the observed brightness of a sloping surface is

$$L = \frac{\rho^{dir} E^{dir} + \rho^{dif} E^{dif}}{\pi} \tag{4}$$

where $L$ is the radiance at the bottom of atmosphere, $\rho^{dir}$ is the surface reflectance for direct light, $E^{dir}$ is the direct irradiance, $\rho^{dif}$ is the surface reflectance for diffuse light, and $E^{dif}$ is the diffuse irradiance (reflectances are implicitly assumed to be in the direction of the observer). Topographic correction requires that we transform sloping surface reflectances to their horizontal surface equivalents. This relationship has been characterized for direct light by Dymond and Shepherd (1999) who write the horizontal surface reflectance for direct light, $\rho_h^{dir}$, as

$$\rho_h^{dir} = \frac{\cos i + \cos e}{\cos i_h + \cos e_h} \rho^{dir} \tag{5}$$

where $i$ and $e$ are the incidence and exitance angles on an inclined surface, and $i_h$ and $e_h$ are the incidence and exitance angles on a horizontal surface (figure 2). As diffuse irradiance tends to be small in comparison with direct irradiance, we make the simplifying assumption that diffuse reflectance is Lambertian, and rewrite equation (4) as

$$L = \frac{\rho_h^{dir} E^{dir}/\gamma + \rho_h^{dif} E^{dif}}{\pi} \tag{6}$$

where $\rho_h^{dif}$ is the horizontal surface reflectance for diffuse light and

$$\gamma = \frac{\cos i + \cos e}{\cos i_h + \cos e_h} \tag{7}$$

In most instances the useful signal received by the satellite comes primarily from reflection of direct light; however, solving equation (6) for $\rho_h^{dir}$ requires calculation of the horizontal diffuse reflectance. Rather than trying to estimate diffuse reflectances for shaded parts of the imagery, we assume that the diffuse reflectance is some

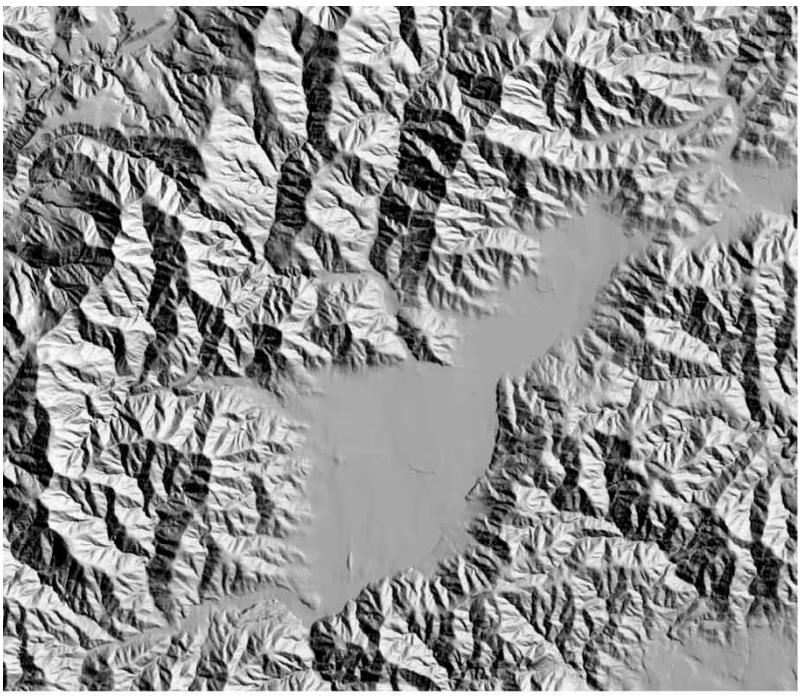

Direct Irradiance

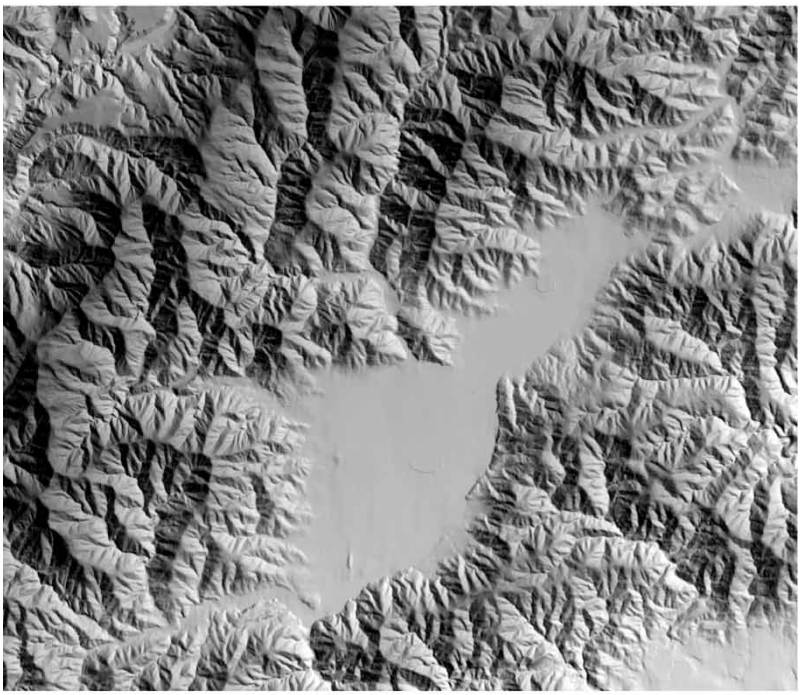

Diffuse Irradiance

Figure 1. Irradiance images for the red spectral band of SPOT 4.

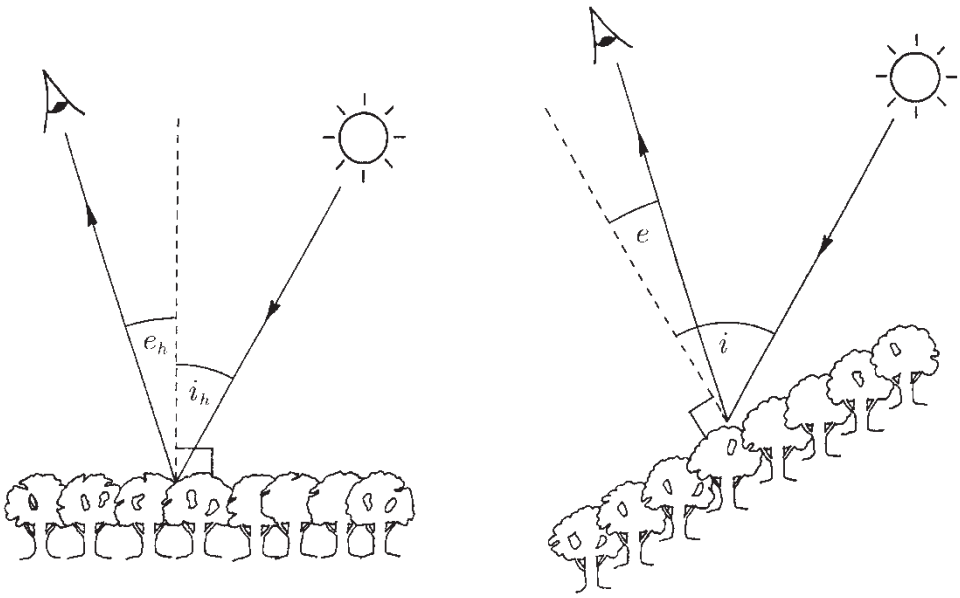


Figure 2. Schematic comparing reflection angles of a vegetation canopy on a horizontal surface with those on an inclined surface. Incidence and exitance angles on the horizontal surface are $i_h$ and $e_h$ and on the inclined surface are $i$ and $e$.

multiple, $\beta$, of the direct reflectance, and solve equation (6) to give the reflectance correction equation

$$\rho_h^{dir} = \frac{\pi L}{E^{dir}/\gamma + \beta E^{dif}} \tag{8}$$

The ratio $\beta$ can be evaluated from a bidirational reflectance model on a case-by-case basis. We calculated $\beta$ from the model of Dymond *et al.* (2001) to be 1.06 for the SPOT 4 image which had a sun elevation of 57°. It is a reasonable approximation to set $\beta = 1$ for moderate sun elevations between 50° and 70°.

The task is then to produce images of direct reflectance of a horizontal surface, an attribute independent of atmosphere and topography. Note that equation (8) involves bottom of atmosphere radiance, so the 6S code is also required to transform top of atmosphere radiance, as directly measured by satellite, to bottom of atmosphere radiance.

## 3. Results

The imagery chosen for investigation was a 20 m resolution SPOT 4 image of a mountainous region of North Canterbury, New Zealand. The DEM used for image orthorectification and topographic correction was derived from a 20 m contour set using a contour growing algorithm (Letts and Rochon 1980). The DEM was first created at 10 m resolution, double smoothed using $3 \times 3$ low pass filters, and then resampled to a 20 m grid to match the SPOT imagery. This process minimizes contour artefacts in the DEM that can have a significant effect on slope and aspect calculations. From the SPOT 4 scene (60 km × 60 km), a mountainous study area of 29 km × 25 km containing a variety of vegetation covers was selected. The irradiance

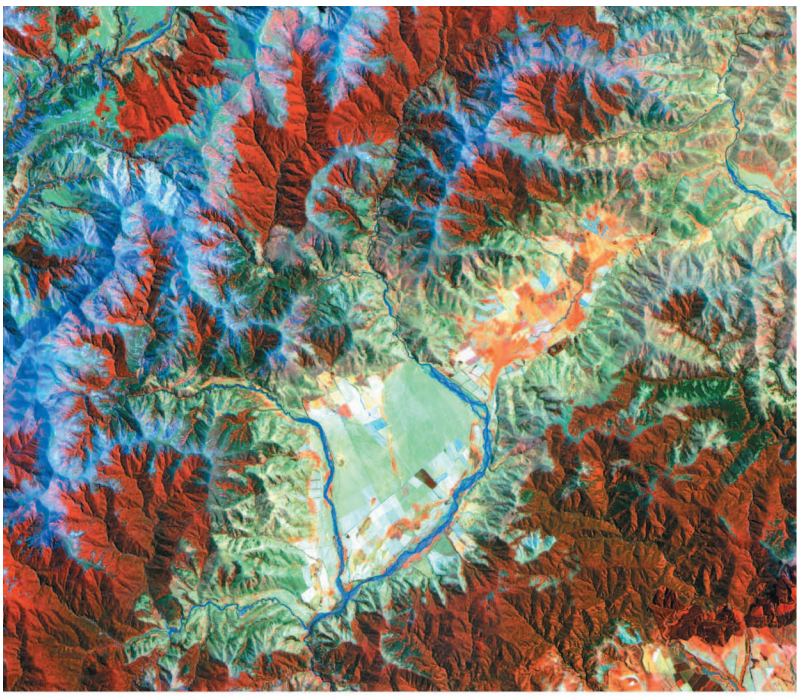

(*a*) Original

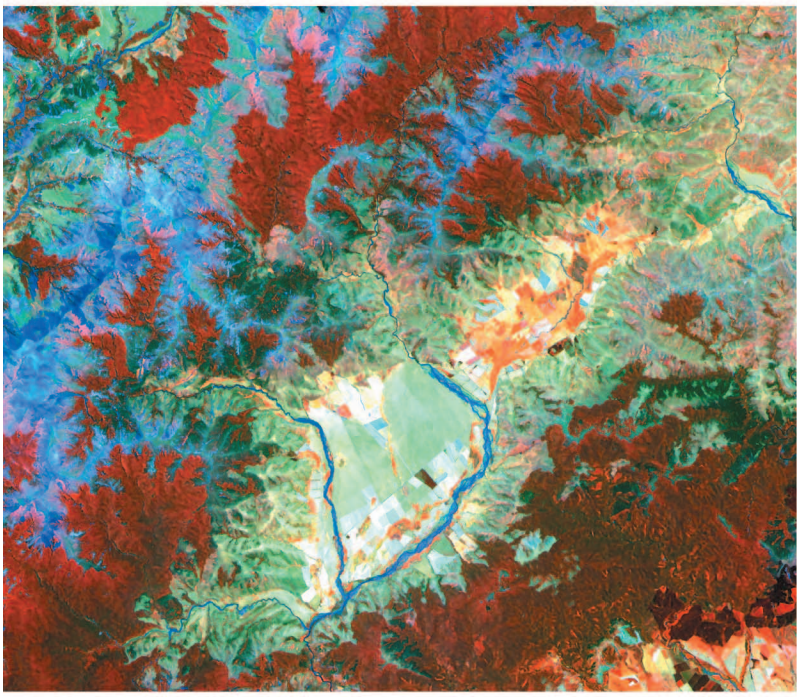

(*b*) Illumination and Reflectance Corrected

Figure 3. Comparison between (*a*) original SPOT 4 image and (*b*) terrain-corrected image.

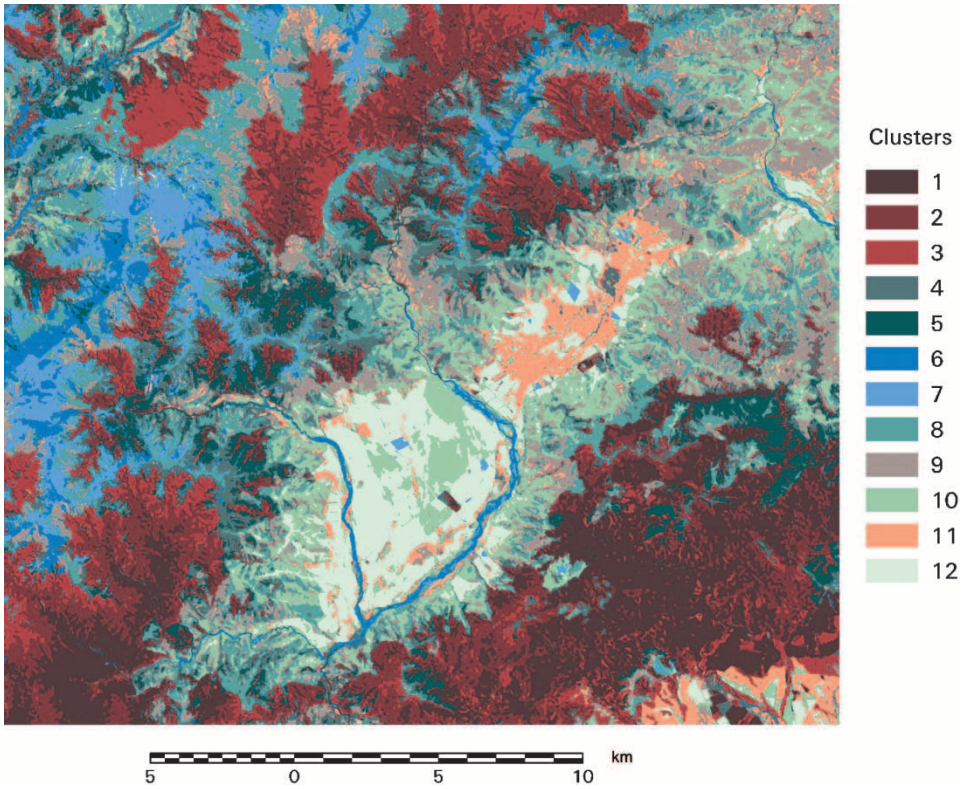


Figure 4. Unsupervised 12-cluster classification.

algorithm outlined in §2.1 was applied for this area and images of direct and diffuse irradiance calculated for each of the four spectral bands (red band images are shown in figure 1). Using the 6S atmospheric code, the raw image was corrected to bottom of atmosphere radiance. DEM slope and aspect were combined with the known solar and view positions to produce an image of the $\gamma$ function (equation (7)). The radiance, irradiance, and $\gamma$ images were then input into equation (8) to perform the illumination and reflectance correction. The comparison between the original reflectance image and the terrain-corrected image is shown in figure 3.

We see from figure 3 that the topographic variability has been removed and the corrected image is a flat surface representation of the original. This observed flattening should produce cleaner spectral signatures; that is, reduced variation in reflectance per vegetation group. To measure this reduced variation, per vegetation group, we performed an unsupervised classification on the corrected image to produce 12 spectral clusters (figure 4) that correspond to broad vegetation groups or bare ground. We then calculated the coefficient of variation (standard deviation divided by the mean) of reflectance for each vegetation group (tables 1–4).

For the full illumination and reflectance correction, the coefficients for clusters 1–10 have large reductions, with respect to the original image, in all spectral bands. Cluster 11 has a small increase in the visible bands, while cluster 12 has a small reduction. These are pasture areas and, as we can see from the average slope of the clusters, are on predominantly flat land where the topographic correction will have

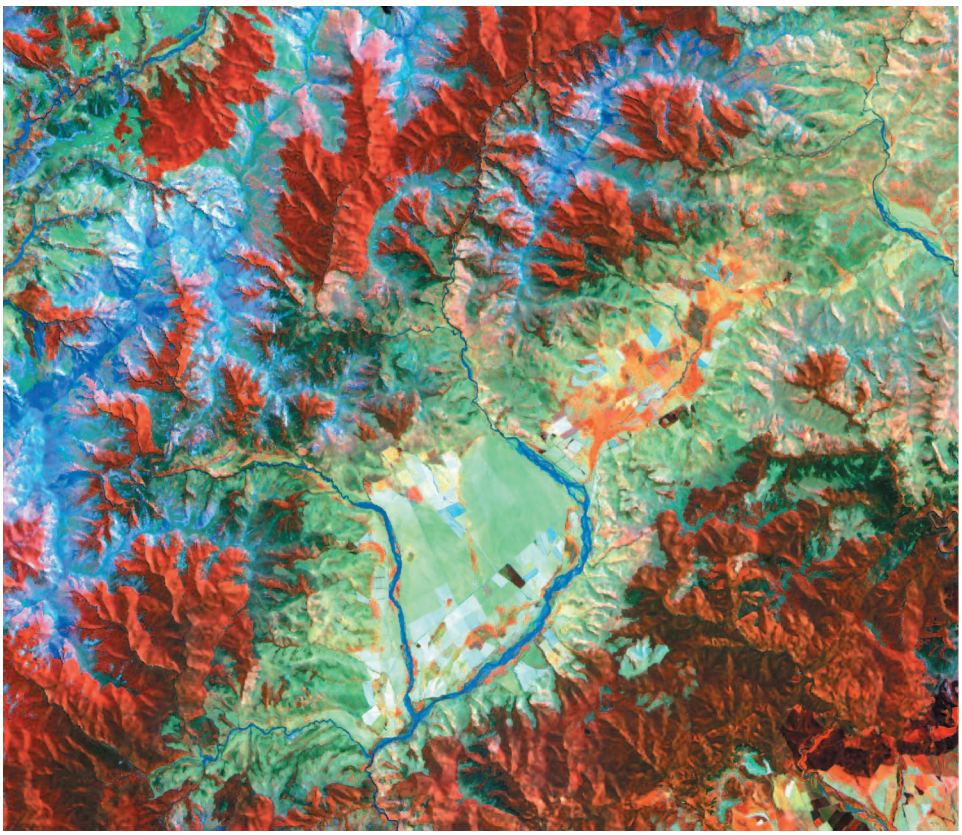

Figure 5. SPOT 4 image corrected for illumination only (equivalent to assuming Lambertian reflectance).

little effect. In contrast, the illumination correction on its own (figure 5) increased the coefficients of variation in most of the clusters for the visible bands, with bare ground having the the only reduction (perhaps it is closer to a Lambertian surface than vegetation). While the illumination correction does succeed in reducing the coefficients of variation in the infrared, it is outperformed by the full illumination and reflectance correction. The increased variation is the visible combined with limited success in the infrared, suggest that performing an illumination correction on its own has little merit.

## 4. Discussion

The method presented in this paper processes satellite imagery, which is essentially top of atmosphere radiance, to bottom of atmosphere reflectance on a level surface. Hence, the satellite signal is converted from a mix of illumination, atmosphere and vegetation reflectance, to vegetation reflectance alone. It is this property that maximizes the information content of satellite imagery. Any changes detected in satellite imagery may then be ascribed to a change in the vegetation. Thus, satellite imagery may be used to monitor the state and health of vegetation in time.

As New Zealand is a very mountainous country, we plan to use the method presented here to improve the automate remote sensing of vegetation. At present,

average monthly values of water vapour, ozone and aerosols are used in the 6S code. Using actual values on the day of image acquisition would improve the method even more. It is unlikely there will be a ground network providing these daily measurements, hence in the future we will be looking to satellite platforms such as TERRA to provide daily data. New Zealand is well covered by digital elevation data with a national coverage of 20 m digital contours. These contours are easily processed to DEMs at 10 or 20 m pixels, and then smoothed to minimize errors in slope.

The success of the method is due to the combination of illumination and reflectance correction. Topography not only affects the illumination of slopes, but significantly changes the reflectance of vegetation as a function of the geometry of sun, target and viewer relative to the slope normal. The correction for reflectance conveniently has no parameters, and may be applied to any vegetation type. When both these effects are corrected, satellite imagery of hilly and mountainous country is completely flattened. The effect is quite dramatic and immediately facilitates much easier visual interpretation. The significant reduction of variance in spectral signatures promises higher mapping accuracies for automatic classification, together with more detailed classifications (i.e. more classes).

## 5. Conclusion

The results in this paper have shown that topographic variation exhibited in satellite imagery can be removed, producing a reduction in the coefficient of variation of spectral signatures. This reduction means that automated classification of features on rugged terrain becomes a realistic proposition. This excellent result is due to the fact that in addition to correcting for illumination, this algorithm corrects for the dependence of vegetation reflectance on slope.

## References

Civco, D. L., 1989, Topographic normalisation of Landsat Thematic Mapper digital imagery. *Photogrammetric Engineering and Remote Sensing*, **55**, 1303–1309.

Conese, C., Gilabert, M. A., Maselli, F., and Bottai, L., 1993a, Topographic normalization of TM scenes through the use of an atmospheric correction method and digital terrain models. *Photogrammetric Engineering and Remote Sensing*, **59**, 1745–1753.

Conese, C., Maracchi, G., and Maselli, F., 1993b, Improvement in maximum likelihood classification performance on highly rugged terrain using principle components analysis. *International Journal of Remote Sensing*, **14**, 1371–1382.

Dymond, J. R., 1988, Nonparametric modeling of radiance in hill country. *Remote Sensing of Environment*, **25**, 3–21.

Dymond, J. R., 1992, Nonparametric modelling of radiance in hill country for digital classification of aerial photographs. *Remote Sensing of Environment*, **39**, 95–102.

Dymond, J. R., and Shepherd, J. D., 1999, Correction of the topographic effect in remote sensing. *IEEE Transactions on Geoscience and Remote Sensing*, **37**, 2618–2620.

Dymond, J. R., Shepherd, J. D., and Qi, J., 2001, A simple physical model of vegetation reflectance for standardising optical satellite imagery. *Remote Sensing of Environment*, **77**, 230–239.

Ekstrand, S., 1996, Landsat TM-based forest damage assesment: correction for topographic effects. *Photogrammetric Engineering and Remote Sensing*, **62**, 151–161.

Fleming, M. D., and Hoffer, R. M., 1979, Machine processing of Landsat MSS data and DMA topographic data for forest cover type mapping. In *Machine Processing of Remotely Sensed Data Symposium*, (West Lafayette, IN, USA: Purdue University), pp. 377–390.

Franklin, S. E., Peddle, D. R., and Moulton, J. E., 1989, Spectral/geomorphometric discrimination and mapping of terrain: a study in Gros Morne national park. *Canadian Journal of Remote Sensing*, **15**, 28–42.

HOLBEN, B. N., and JUSTICE, C. O., 1980, The topographic effect on spectral response from nadir-pointing sensors. *Photogrammetric Engineering and Remote Sensing*, **49**, 1191–1200.

HUGLI, H., and FREI, W., 1983, Understanding anisotropic reflectance in mountainous terrain. *Photogrammetric Engineering and Remote Sensing*, **49**, 671–683.

HUTCHINSON, C. F., 1982, Techniques for combining landsat and ancillary data for digital classification improvement. *Photogrammetric Engineering and Remote Sensing*, **48**, 123–130.

JUSTICE, C. O., WHARTON, S. W., and HOLBEN, B. N., 1981, Application of digital terrain data to quantify and reduce the topographic effect on Landsat data. *International Journal of Remote Sensing*, **2**, 213–230.

KONDRATYEV, K. Y., 1969, *Radiation in the Atmosphere* (London: Academic Press).

LEPRIEUR, C. E., DURAND, J. M., and PEYRON, J. L., 1988, Influence of topography on forest reflectance using Landsat thematic mapper and digital terrain data. *Photogrammetric Engineering and Remote Sensing*, **54**, 491–496.

LETTS, P. J., and ROCHON, G., 1980, Generation and use of digital elevation data for large areas. In *6th Canadian Symposium on Remote Sensing*, (Halifax, Nova Scotia: Canadian Remote Sensing Society), pp. 597–602.

MEYER, P., ITTEN, K. I., KELLENBERGER, T., SANDMEIER, S., and SANDMEIER, R., 1993, Radiometric corrections of topographically induced effects on Landsat TM data in an alpine environment. *ISPRS Journal of Photogrammetry and Remote Sensing*, **48**, 17–28.

PELLIKKA, P., 1996, Illumination compensation for aerial video images to increase land cover classification accuracy in mountains. *Canadian Journal of Remote Sensing*, **22**, 368–381.

PROY, C., TANRÉ, D., and DESCHAMPS, P. Y., 1989, Evaluation of topographic effects in remotely sensed data. *Remote Sensing of Environment*, **30**, 21–32.

RICHTER, R., 1997, Correction of atmospheric and topographic effects for high spatial resolution satellite imagery. *International Journal of Remote Sensing*, **18**, 1099–1111.

ROBERTS, P. A., 1981, The use of terrain height information with satellite imagery. In *Matching Remote Sensing Technologies and their Applications* (London: Remote Sensing Society), pp. 317–327.

SANDMEIER, S., and ITTEN, K., 1997, A physically-based model to correct atmospheric and illumination effects in optical satellite data of rugged terrain. *IEEE Transactions on Geoscience and Remote Sensing*, **35**, 708–717.

SENOO, T., KOBAYSHI, F., TANAKA, S., and SUGIMURA, T., 1990, Improvement of forest type classification by SPOT HRV with 20 m mesh DTM. *International Journal of Remote Sensing*, **11**, 1011–1022.

SMITH, J. A., LIN, T. L., and RANSON, K. J., 1980, The Lambertian assumption and Landsat data. *Photogrammetric Engineering and Remote Sensing*, **46**, 1183–1189.

STOHR, C. J., and WEST, T. R., 1975, Terrain and look angle effects upon multispectral scanner response. *Photogrammetric Engineering and Remote Sensing*, **51**, 229–235.

TEILLET, P. M., 1986, Image correction for radiometric effects in remote sensing. *International Journal of Remote Sensing*, **7**, 1637–1651.

TEILLET, P. M., GUINDON, B., and GOODENOUGH, D. G., 1982, On the slope-aspect correction of multispectral scanner data. *Canadian Journal of Remote Sensing*, **8**, 84–106.

THOMSON, A. G., and JONES, C., 1990, Effects of topography on radiance from upland vegetation in North Wales. *International Journal of Remote Sensing*, **11**, 829–840.

TROTTER, C. M., 1998, Characterizing the topographic effect at red wavelengths using juvenile conifer canopies. *International Journal of Remote Sensing*, **19**, 2215–2221.

VERMOTE, E., TANRÉ, D., DEUZÉ, J. L., HERMAN, M., and MORCRETTE, J. J., 1997, Second Simulation of the Satellite Signal in the Solar Spectrum (6S). NASA Goddard Space Flight Center, Greenbelt, MD, USA.

WOODHAM, R. J., and GRAY, M. H., 1987, An analytic method for radiometric correction of satellite multispectral scanner data. *IEEE Transactions on Geoscience and Remote Sensing*, **25**, 258–271.